HHS Public Access

Author manuscript

Methods Enzymol. Author manuscript; available in PMC 2020 July 18.

Published in final edited form as:

Methods Enzymol. 2019 ; 626: 561–585. doi:10.1016/bs.mie.2019.06.029.

Preparation of a New Construct of Human Histone Deacetylase 8 for the Crystallization of Enzyme-Inhibitor Complexes

Nicholas J. Porter, **David W. Christianson***

Roy and Diana Vagelos Laboratories, Department of Chemistry, University of Pennsylvania, Philadelphia, Pennsylvania, 19104–6323, United States

Abstract

The metal-dependent histone deacetylases (HDACs) are critical regulatory enzymes that modulate myriad cellular processes. Implicated in cancer, neurodegenerative diseases, and other clinical disorders, various HDAC isozymes serve as validated drug targets. However, structural similarities among the HDAC isozymes challenge efforts in targeting a single isozyme for therapeutic intervention with an inhibitor. X-ray crystallography remains the premiere technique for studying the chemistry of isozyme-selective inhibition. While crystal structures of many HDAC-inhibitor complexes have been determined, especially with the class I isozyme HDAC8, the study of complexes with large inhibitors is complicated by flexible regions of the protein structure that can hinder crystallization. Here, we outline an approach for the identification of regions in HDAC8 that may hinder crystallization. We also describe protocols for the design and preparation of a truncated HDAC8 construct, $HDAC8_{374}$, that enabled the successful crystallization and structure determination of the HDAC8–Trapoxin A complex at 1.24 Å resolution.

Keywords

zinc enzyme; epigenetics; protein crystallography; drug design

1. Introduction

Post-translation lysine acetylation is a crucial regulatory mechanism for modulating enzyme function within the cell (Wang et al., 2010; Zhao et al., 2010; Choudhary et al., 2014). Following Allfrey's discovery of histone acetylation and its role in transcriptional regulation more than 50 years ago (Allfrey et al., 1964), almost 40,000 acetylation sites have been identified in the mammalian proteome (Hornbeck et al., 2014). However, there are only 18 enzymes, known as histone deacetylases (HDACs) or lysine deacetylases (KDACs), capable of reversing this modification (Ellmeier & Seiser, 2018). Therefore, each HDAC must have multiple protein substrates *in vivo*, with activity against these substrates regulated by the formation of large multi-protein complexes, cellular conditions, and/or other chemical factors.

*Corresponding author: chris@sas.upenn.edu.

Dysregulation of HDAC activity is linked to numerous diseases including cancer, neurodegenerative disorders, and developmental impairments (Abend & Kehat, 2015; Sharma & Taliyan, 2015; Ferrari et al., 2018). Certain HDAC isozymes have been validated as drug targets for the treatment of some of these diseases (Dokmanovic et al., 2007; Gupta et al., 2012; Falkenberg & Johnstone, 2014; Ganai et al., 2016). However, structural similarities among different HDACs complicate the design of therapeutics targeting a single isozyme. Consequently, therapies targeting the inhibition of one HDAC isozyme can result in serious off-target effects due to the inhibition of other unintended isozymes (Benedetti et al., 2015). Among the four phylogenetic classes of HDACs, classes I, II, and IV comprise the metal-dependent HDACs. These enzymes adopt a topologically identical fold to that first observed in rat liver arginase (Kanyo et al., 1996; Ash et al., 2000). Accordingly, this fold is designated the arginase-deacetylase fold (Gregoretti et al., 2004; Lombardi et al., 2011).

For the development of more effective therapeutics targeting the inhibition of metal-dependent HDACs, the structural characterization of HDAC-inhibitor complexes guides the design of drug screening libraries. To date, many human HDAC8-inhibitor complexes have been structurally characterized (Somoza et al., 2004; Vannini et al., 2004, 2007; Dowling et al., 2008, 2010; Cole et al., 2011; Whitehead et al., 2011; Decroos et al., 2014, 2015a,b; Gantt et al., 2016; Tabackman et al., 2016; Porter et al., 2016, 2017; Marek et al., 2018). The majority of these complexes involve single-point mutants of HDAC8 identified in children diagnosed with Cornelia de Lange Syndrome (Deardorff et al., 2012, 2016; Kaiser et al., 2014). While these structures provide insight regarding HDAC8 function, interactions of residues distant from the active site are known to influence biological function (Castaneda et al., 2017). Therefore, new approaches that will enable the characterization of such long-range interactions are vital for the development of selective HDAC8-targeted therapies. Protein substrates of HDAC8 include SMC3 in the cohesin complex, the tumor suppressor ARID1A, and more than 100 additional nuclear and cytosolic proteins involved in cellular regulation and homeostasis, chromatin remodeling, transcriptional regulation, RNA splicing, and cytoskeleton function (Olson et al., 2014; Lopez et al., 2017). Newly identified protein substrates of HDAC8 may implicate this isozyme as a potential drug target as new regulatory pathways are explored.

Here, we describe a new construct of human HDAC8, designated $HDAC8_{374}$, that can be used for cocrystallization of enzyme-inhibitor complexes. The design of this construct was motivated by the observation that full-length human HDAC8 generally crystallizes as a dimer in which intermolecular contacts are made between loops flanking the active site of each monomer. These packing interactions in the crystal lattice hinder the binding and crystallization of complexes with larger inhibitors and substrates. Of the 47 structures of human HDAC8 determined to date (Table 1), this crystal lattice packing phenomenon is observed in 39 structures (Figure 1). The protocol outlined in this chapter leading to the design and preparation of $HDAC8_{374}$, which is not as susceptible to crystallization as a dimer and hence can accommodate larger inhibitors, enabled the successful crystallization and structure determination of the HDAC8–Trapoxin A complex at 1.24 Å resolution (Porter & Christianson, 2017). Trapoxin A is a microbial cyclic tetrapeptide bearing an unusual α,β-epoxyketone side chain (Itazaki et al., 1990), the ketone carbonyl group of which is isosteric with the amide carbonyl of the HDAC8 substrate acetyllysine. The crystal structure of the

HDAC8–Trapoxin A complex revealed that the ketone carbonyl of Trapoxin A undergoes nucleophilic attack to bind as a gem-diolate, as similarly observed for the binding of ketonic substrate analogues to other zinc hydrolases (Christianson et al., 1987; Hai & Christianson, 2016).

2. Analysis of Crystal Packing Interactions

Protein crystal packing is easily assessed using standard structure analysis tools such as PyMOL (DeLano, 2002) or UCSF Chimera (Pettersen et al., 2004). The method presented here uses the free-to-download Educational-Use-Only build of PyMOL, which can be installed on a desktop or laptop computer. Instructions for downloading the software are also included. Crystal packing is assessed at two levels: (1) interactions between multiple monomers within the asymmetric unit and (2) interactions between adjacent unit cells. Analysis of these interactions in the crystal structure of the HDAC8-Largazole complex (PDB 3RQD; Cole et al., 2011) guided the design of the new HDAC8 construct for cocrystallization with Trapoxin A.

2.1 Download and Installation of the Educational-Use-Only PyMOL Build

1. Go to https://pymol.org.edu/?q=educational/.
2. Enter relevant information including your name, email address, and institution.
3. An e-mail will be sent containing the username and password for access to the PyMOL download URL.
4. Go to: http://pymol.org/ep and enter the credentials provided in the e-mail.
5. For the installation of PyMOL 2.0, download the License File provided and then proceed by clicking the link to the “PyMOL Download Page”.
6. Select the PyMOL installer for the appropriate operating system. This will begin downloading the application.
7. Once the download is complete, open PyMOL and provide the license file downloaded in Step 5. The Educational-Use-Only build of PyMOL will now be activated.

2.2 Visualization of Crystal Packing Interactions

1. Open PyMOL and use the command fetch XXXX in the PyMOL terminal at the top of the interface to load the structure with PDB ID XXXX.
    a. Example: the command fetch 3RQD will load the structure of the HDAC8-Largazole complex as shown below (Figure 2).
    b. Note: it is often helpful to remove hydrogen atoms (if present) and solvent molecules from the structure using the remove hydro and remove solvent commands, respectively. This will reduce the amount of processing needed in subsequent steps.

2. To generate symmetry mates, use the command symexp prefix, object, selection, cutoff, substituting the appropriate terms as defined below.
    a. prefix – provides the name for the symmetry mates generated as new objects
    b. object – name of the object for which symmetry mates will be generated. The PDB ID of the structure can be inserted here.
    c. selection – atom selection from which the cutoff distance will be measured (Å). To generate symmetry mates in all directions from the asymmetric unit, enter the PDB ID again here.
    d. cutoff – distance (Å) from the selection within which any symmetry mates will be generated. Generally, a value of 3–10 Å can be used to generate all first-shell symmetry mates.
    e. Example: the command symexp 3RQDsym, 3RQD, 3RQD, 10 will generate 10 symmetry mates around the crystallographic dimer loaded in Step 1. Using the command hide followed by show surface will display the surfaces of each asymmetric unit (Figure 3).
3. Voids in the crystal lattice surrounding the asymmetric unit will be readily apparent (indicated by red arrows in Figure 3). The following structural features near these voids can be studied for the design of an optimized construct for crystallography:
    a. Polypeptide chain termini – Check the N- and C-terminal residues in the structure. These commonly contain disordered segments and are oriented near voids. Compare the resolved amino acids to the FASTA sequence found under “Display Files” in the PDB entry. If the first residue observed in the structure is not the first residue in the sequence, then a disordered peptide is accommodated within the adjacent void. Unstructured residues can be truncated to generate a more ordered construct.
    b. Loops – If there are gaps in the sequence of the observed structure, this indicates the presence of a disordered loop that occupies an adjacent void. Such loops can be substituted with a glycine-serine linker spanning the distance between the residues resolved on either end of the loop.
4. After identifying unstructured amino acids that occupy voids in the lattice, a construct can be designed that contains less disorder and is therefore likely to be more amenable to crystallography.

2.3 Notes

When removing disordered portions of a protein to optimize crystallization properties, the polypeptide chain termini should be targeted first. The removal or truncation of loops may complicate protein expression or purification, and multiple constructs may have to be

generated before an optimal construct is identified for crystallization. For HDAC8, this analysis revealed that the first and last structured residues in the HDAC8-Largazole complex are L14 and V377; both are located adjacent to voids in the crystal lattice. The HDAC8 construct in this crystal structure consists of full-length HDAC8 (residues 1–377) followed by a Factor Xa cleavage site and a C-terminal hexahistidine tag, meaning that 25 residues are disordered at the polypeptide chain termini. With the rationale that these disordered segments could hinder crystallization in alternative packing arrangements, the following protocols were used to generate, express, purify, and crystallize a new truncated HDAC8 construct in complex with Trapoxin A (Porter & Christianson, 2017).

3. Ligation-Independent Cloning of a Truncated Protein Construct

Ligation-Independent Cloning (LIC) is a fast and effective technique for the insertion of a gene into a LIC-templated plasmid (Aslanidis & de Jong, 1990). Many LIC plasmids bearing different expression tags are available from the Scott Gradia Lab through Addgene (https://www/addgene/org/Scott_Gradia). For the truncation construct of HDAC8, a vector containing an N-terminal hexahistidine tag followed by maltose binding protein (MBP) and a tobacco etch virus (TEV) protease cleavage site was selected.

3.1 Equipment

1. T100™ Thermal Cycler (Bio-Rad #1861096)
2. Microwave oven for preparation of agarose gel
3. Mini-Sub® Cell GT Complete gel casting system (Bio-Rad #1704486)
4. Mini-Sub® Cell GT electrophoresis cell (Bio-Rad #1704487)
5. EC-3000P series 90 programmable electrophoresis power supply (or comparable; Thermo Scientific)
6. Transilluminator FBTIV-88 (or comparable; Fischer Scientific)
7. Thermal-Lok Dry Heat Bath (USA Scientific #2510-1101)
8. MiniSpin® plus centrifuge (Eppendorf #022620207)
9. Milli-Q® Integral Water Purification System for Ultrapure Water (EMD Millipore #ZRXQ003WW)
10. Isotemp™ waterbath (Fisher Scientific #15-462-S2)
11. New Brunswick™ Innova® 40R benchtop incubator shaker (Eppendorf #M1299-0094)
12. 37°C incubator for microbiological culture

3.2 Materials

1. 200 μL thin-walled PCR tubes (BRAND #781305)

2. 10 ng/μL sample of plasmid containing the *H. sapiens* (human) HDAC8 gene (codon optimized; residues 1–377); obtained from the previously described HDAC8-His_6-pET20b construct (Dowling et al. 2008).
3. 3 μg sample of pET His6 MBP TEV LIC vector encoding a TEV protease-cleavable N-terminal hexahistidine-MBP tag (from Dr. Scott Gradia, University of California; Berkeley; Addgene #29656)
4. 100 μM stocks of oligonucleotide primers for the PCR amplification of truncated HDAC8 (residues 8–374) with LIC tag primer sequences
    a. Forward LIC tag primer: 5'–TACTTCCAATCCAATGCA…"
    b. Reverse LIC tag primer: 5'–TTATCCACTTCCAATGTTATTA…"
    c. After the above sequences, add nucleotides sequences with 14–18 base pairs of complementarity to each end of the gene to be inserted in the vector. The melting temperatures of these primers should be within 5°C of one another.
5. 10 nM deoxynucleotide triphosphate (dNTP) mixture, PCR grade (Invitrogen #18427013)
6. 2.5 unit/μL stock of *PfuUltra* High-Fidelity DNA Polymerase (Agilent Technologies #600380)
7. Agarose powder (Fischer BP1356)
8. 1x Tris-acetate-EDTA (TAE) buffer, provided as a 50X stock (Bio-Rad #1610743)
9. SYBR™ Safe DNA gel stain, provided as 10,000X stock (Invitrogen #S33102)
10. Purple gel loading dye, provided as 6X stock (New England BioLabs #B7024S)
11. 100 bp DNA ladder (New England BioLabs #N3231S)
12. 1.5-mL microcentrifuge tubes (Fisherbrand #05-408-129)
13. CutSmart® buffer, provided as 10X stock (New England BioLabs #B7240S)
14. SspI-HF restriction endonuclease (New England Biolabs #R3132S)
15. QIAquick PCR Purification Kit (QIAGEN #28104)
16. NEBuffer™ 2.1 (New England BioLabs #B7202S)
17. Deoxycytidine triphosphate (dCTP; Invitrogen #10217016)
18. Deoxyguanosine triphosphate (dGTP; Invitrogen #10218014)
19. Dithiothreitol (GoldBio #DTT50)
20. Bovine Serum Albumin (Sigma Aldrich #A9418)
21. T4 DNA polymerase (New England BioLabs #M0203S)

22. Ethylenediamine tetraacetic acid (EDTA), disodium salt, dihydrate (Fisher Scientific #BP120)
23. NEB® 5α competent *E. coli* (High Efficiency) (New England BioLabs #C2987I)
24. LB agar plates with 50 mg/mL kanamycin
25. LB broth, Miller (Sigma Aldrich #L3152)
26. QIAquick PCR Purification Kit (QIAGEN #27104)

3.3 Procedure

1. Prepare a 50 μL PCR sample in a 200-μL PCR tube with the following final concentrations:
   a. 0.2–0.4 ng/μL of template plasmid DNA (HDAC8-His_6-pET20b; 10–20 ng total)
   b. 0.5 μM of forward and reverse LIC primers
   c. 0.25 mM dNTP mixture
   d. 0.05 units/μL *PfuUltra* High-Fidelity DNA Polymerase (1 μL of 2.5 units/μL stock).

   Note: keep stock on ice or at −20°C at all times to avoid loss of activity.
2. Program the T100™ Thermal Cycler for the following run protocol (run time = 192 min):

1 cycle:	95°C / 2 min
40 cycles:	95°C / 30 s
	57°C / 2 min
	72 °C / 2 min
1 cycle:	72°C / 10 min
hold:	20°C

3. Place the 200-μL PCR tube into the T100™ Thermal Cycler and run the above program.
4. Once the sample has finished, prepare a 1.0% (w/v) agarose gel using 1x Tris-acetate-EDTA buffer by dissolving the agarose in buffer in the microwave (50 mL is sufficient for a standard size gel). When warm but not burning to the touch, add SYBR™ Safe stain to 1x concentration and pour into casting tray with appropriately sized comb.
5. When PCR is complete, prepare the following 6 μL samples:
   a. 100 bp DNA ladder – dilute 1 μL of ladder with 4 μL of H_2O and 1 μL of 6X gel loading dye
   b. PCR sample – add 1 μL of 6X gel loading dye to 5 μL of 50 μL PCR reaction

6. Remove comb from gel and transfer cast gel into the electrophoresis system, submerging the gel in 1X TAE buffer. Apply samples from Step 5 to separate wells of gel. Be sure to orient the gel correctly so that the bands will migrate into the gel and not out into the reservoir.
7. Run the agarose gel at 100 V for 40 min.
8. When complete, visualize the gene insert band using the transilluminator. If a band is observed corresponding to the correct number of bp, then set the remaining 45 μL aside while vector is prepared.
9. For vector linearization, prepare a 100 μL digestion sample in a 1.5 mL microcentrifuge tube with the following concentrations:
    a. 30 ng/μL of pET His6 MBP TEV LIC vector (3 μg total)
    b. 1X CutSmart® buffer
    c. 0.6 units/μL SspI-HF (3 μL of 20 units/μL stock). Note: keep stock on ice or at −20°C at all times to avoid loss of activity.
10. Incubate digestion reaction at 37°C for 1 h using the dry heat bath.
11. When complete, perform a PRC clean-up on both the linearized vector and the gene insert using the procedure provided with the QIAquick PCR Purification Kit.
12. For the T4 polymerase digestions, which will generate complementary sticky ends on the vector and insert, prepare two separate 40-μL reactions as follows:
    a. 4 μL of 10X NEBuffer™ 2.1
    b. 30 μL of linear DNA (either vector OR insert)
    c. 1 μL of 100 mM dNTP (dGTP for the vector or dCTP for the insert)
    d. 2 μL of 100 mM dithiothreitol
    e. 2 μL of 10 mg/mL bovine serum albumin (BSA)
    f. 1 μL of 3 units/μL T4 DNA polymerase
13. Incubate reactions at room temperature for 30 min.
14. Heat reactions at 75°C for 20 min using the digital dry bath. This precipitates the T4 DNA polymerase.
15. Centrifuge reactions at 14,000 rpm (13,000*g*) at 4°C using the MiniSpin® plus centrifuge.
16. Remove the supernatant and perform an ethanol precipitation to precipitate digested DNA.
17. Redissolve vector and insert in 12 μL of ultrapure water from MilliQ® system.
18. Set up 1:0, 1:1, 1:2, 1:3, and 1:4 volume ratios of vector:insert to maximize cloning efficiency. The 1:0 solution will serve as a negative control. It is

recommended to maintain 1 μL of vector and 1 μL, 2 μL, 3 μL, and 4 μL of insert for the other ratios.

19. Incubate the vector:insert reactions at room temperature for 30 min.
20. Add 1 μL of 25 mM EDTA.
21. Incubate all reactions at room temperature for an additional 15 min.
22. Add the full volume of each ratio mixture to separate 50 μL NEB® 5α *E. coli* aliquots
23. Incubate cells on ice for 30 min.
24. Heat shock the cells for 40–45 s at 42°C using the Isotemp waterbath.
25. Immediately return the cells to ice and incubate for 10 minutes
26. Add 300 μL of SOC media (comes with commercial stock of NEB® 5α cells. Note: if SOC media is not available, then standard LB is also acceptable).
27. Incubate tubes in Innova 40R shaker at 37°C for 1 h.
28. Plate all 350 μL of each aliquot of cells on LB-kanamycin plates and incubate at 37°C overnight (15–16 h). Note: plates should be placed with the cover facing down to avoid negative effects from condensation on the lid.
29. Colonies should appear on all plates except the 1:0 ratio control. Grow 5-mL cultures in LB and minprep the DNA by following the instructions provided with the QIAprep Spin Miniprep Kit.
30. Submit these samples to local DNA sequencing centers using T7 promoter and T7 terminator primers, as well as any other internal primers that may be necessary for full sequence coverage. Verify DNA sequence and set plasmids aside for expression.

3.4 Notes

The pET His6 MBP TEV LIC vector was chosen due the additional affinity handle provided by maltose binding protein. Since LIC appends a Ser-Asn-Ala sequence to the N-terminus of the protein encoded by the inserted transcript, the HDAC8 construct included residues 8–374 in which Ala8 was aligned with the Ala of this SNA sequence. This also provides 5–6 residues of disorder between the TEV protease cleavage site and the first structured amino acid of HDAC8, facilitating access of the protease to the digestion site. Since residues 375–377 of HDAC8 are disordered in some structures, these residues were also omitted from the final construct. Accordingly, this new HDAC8 construct is designated "$HDAC8_{374}$". The $HDAC8_{374}$ plasmid is available through Addgene (#122174).

4. Expression and Purification of the $HDAC8_{374}$ Construct

The following expression protocol is adapted from the previously described methods for HDAC8 (Dowling et al., 2008) and the purification protocol is adapted from that described for a similar construct of catalytic domain 2 of HDAC6 from *Danio rerio* (Porter et al.,

2017). This purification scheme isolates HDAC8 with fewer trace impurities than previously described protocols.

4.1 Equipment

1. Milli-Q® Integral Water Purification System for Ultrapure Water (EMD Millipore; #ZRXQ003WW)
2. 12 × 2-L and 1 × 1-L baffled flasks
3. Aluminum foil
4. AMSCO® 250LS Small Steam Sterilizer (STERIS Healthcare)
5. New Brunswick™ Innova® 40R benchtop incubator shaker (Eppendorf #M1299-0094)
6. CO8000 Cell Density Meter (Biochrom #80-3000-45)
7. Sorvall™ LYNX 6000 Superspeed Centrifuge (Thermo Fisher #75006590)
8. Revco® Ultima PLUS −80°C freezer (or comparable; Thermo Scientific)
9. Vortex-Genie 2 (Scientific Industries #IS-0236)
10. 250 mL stainless steel beaker
11. Q700 Sonicator (Qsonica #Q700-110)
12. Econo-Column® glass column with flow adaptor (Bio-Rad #7371522)
13. ÄKTAprime plus FPLC (GE Healthcare #11001313)
14. XCell SureLock™ Mini-Cell (Invitrogen #EI0001)
15. PowerPac™ basic power supply (Bio-Rad #1645050)
16. Sorvall™ ST 16R centrifuge (Thermo Scientific #75004381)
17. HiLoad™ 26/600 Superdex 200 pg gel filtration column (GE Healthcare #28989336)
18. Cary 60 UV-Vis Spectrophotometer (Agilent #G6860A)

4.2 Materials

1. BL21 (DE3) competent *E. coli* (New England BioLabs #C2527I)
2. Casamino acids (Fisher Scientific #BP1424)
3. Difco™ M9 minimal salts, 5x (BD #248510)
4. LB broth, Miller (Sigma Aldrich #L3152)
5. Kanamycin monosulfate, USP grade (GoldBio #K-120-5)
6. D(+)-glucose, ACS reagent, anhydrous (ACROS Organics #410950050)
7. Magnesium sulfate anhydrous (Fisher Scientific #M65-500)

8. Calcium chloride dihydrate, ACS grade (Fisher Scientific #C79-500)
9. 2.0 M Zinc chloride (Hampton Research #HR2-811)
10. Isopropyl β-D-1-thiogalactopyranoside (IPTG) (GoldBio #I2481C)
11. Tris hydrochloride (Thermo Scientific #AAJ2267636)
12. Potassium chloride, ACS grade (Fisher Scientific #P217-500)
13. Tris-(2-carboxyethyl)-phosphine hydrochloride (TCEP HCl) (GoldBio #TCEP25)
14. Glycerol (Sigma Aldrich #G7893)
15. Steritop™ Filter Units with matching 1-L bottles (EMD Millipore #SCGPT05RE)
16. Deoxyribonuclease I, bovine pancreas (Alfa Aesar #J62229)
17. Lysozyme (MP Biomedicals #100834)
18. cOmplete™ protease inhibitor tablets (Roche #11873580001)
19. Amylose resin high flow (New England Biolabs #E8022S)
20. 150-mL Superloop (GE Healthcare #18-1023-85)
21. Tobacco etch virus (TEV) protease (express from Addgene plasmid #pRK793)
22. Spectra/Por® 1 Regenerated Cellulose (RC) Dialysis Tubing (Spectrum #132665)
23. Ni-NTA Agarose (QIAGEN #30210)
24. NuPAGE™ 4–12% Bis-Tris Gel (Invitrogen #NP0323)
25. 1x MES-SDS Running Buffer, provided as a 20X stock (Invitrogen #NP0002)
26. Amicon® Ultra Centrifugal Filters – 10k molecular weight cut-off (EMD Millipore #UFC901024)

4.3 Procedure

1. Transform BL21 (DE3) strain *E. coli* using 1 μL of the plasmid (10 ng/μL) isolated in Section 3. Follow steps 22–28 of section 3.4, substituting LB media for SOC media.
2. Prepare 12 L of M9 minimal media as follows:
    a. 1 L of ultrapure water from MilliQ system (Note: adding water first will prevent media powder from pluming when added to flask)
    b. 5.0 g of casamino acids
    c. 11.7 g of M9 minimal salts
3. Additionally, prepare 500 mL of LB for the starter culture.
4. Seal all flasks with aluminum foil and autoclave at 121°C for 15 minutes.

5. When warm to the touch, but not burning, add 500 μL of 50 mg/mL kanamycin to 500 mL of LB.

6. Inoculate this flask with a single colony of transformed BL21 (DE3) *E. coli*. Incubate this culture overnight (15–16 hours) in a shaker at 37°C and 250 rpm.

7. The following morning, add the following to each flask of M9 minimal media:

   a. 2 g glucose (this serves as a carbon source and also suppresses expression of endogenous maltose binding protein)

   b. 800 μL of 2.5 M $MgSO_4$

   c. 50 μL of $CaCl_2$

   d. 1 mL 50 mg/mL kanamycin

8. Inoculate each flask with 20 mL of starter culture and incubate flasks in shaker at 37°C and 250 rpm.

9. After 2 h, check the OD_{600} every 20 min. When OD_{600} reaches ~1.0, set the shaker temperature to 18°C and allow to cool for 30 minutes.

10. Supplement each flask with 100 μL of 1 M IPTG and 100 μL of 2.0 M $ZnCl_2$. Incubate flasks in shaker at 18°C and 250 rpm overnight (~18–21 h).

11. The following morning, spin down cells at 6,000 rpm (8,000*g*) for 15 min and store pellet (~60 g) at −80°C until prepared for purification. Note: the cell pellet can be used immediately for purification, but a single freeze/thaw cycle assists with efficient cell lysis.

12. Before beginning the purification, make and filter the following buffers:

Buffer A:	Buffer B:
50 mM Tris (pH 8.0)	Buffer A + 10 mM maltose
300 mM KCl	
10% glycerol	
1 mM TCEP	

13. Resuspend cell pellet in 120 mL of Buffer A. This can be done by vortexing the cell pellet in 20–30 mL of buffer at a time, pouring the suspension into a metal beaker on ice, and then stirring the solution at 4°C. Supplement suspension with 0.5 mg/mL lysozyme, 0.1 mg/mL DNase I, and 2 protease inhibitor tablets.

14. Lyse the cells by sonication for 9 min (1 s ON:2 s OFF for a total time of 27 min) at 40% amplitude, pausing the sonicator and mixing occasionally.

15. Spin down the lysate at 18,000 rpm (41,500*g*) for 1 h. Meanwhile, equilibrate a 30-mL amylose column with Buffer A.

16. Transfer clarified lysate to 150-mL Superloop and apply to equilibrated amylose column at 1 mL/min. Note: the addition of lysozyme in the lysis step results in fine cell debris that can resuspend very easily if disturbed. This can be avoided by carefully transferring clarified fraction using a serological pipette.

17. When the signal is reduced to ~50 mAu, elute protein with 100% Buffer B (10 mM maltose). An example of the final chromatogram for this column is presented in Figure 4.

18. Pool eluted fractions (~30–40 mL) and supplement with TEV protease to a final concentration of ~0.2–0.3 mg/mL.

19. Dialyze digestion solution against 1 L of Buffer A at 4°C overnight. If white precipitate forms overnight, it is likely to be TEV protease.

20. The next morning, make the Ni-NTA Elution Buffer which consists of Buffer A supplemented with 400 mM imidazole.

21. Apply the digested protein sample to a Ni-NTA column at 1 mL/min. This should result in a flow-through and a ~50 mL peak plateauing at ~50–100 mAu. This peak contains the TEV protease-digested $HDAC8_{374}$ (Figure 5).

22. Elute hexahistidine-tagged MBP and TEV protease with 400 mM imidazole. An example of the final chromatogram for the Ni-NTA column is presented in Figure 5.

23. Use SDS-PAGE to verify purity of $HDAC8_{374}$ and confirm the removal of MBP and TEV protease. Note: the removal of MBP at this step is key because it is just slightly larger than $HDAC8_{374}$ (MW_{MBP} = 43 kDa; $MW_{HDAC8374}$ = 41 kDa). If separation is less than satisfactory, run the flow-through fractions over the Ni-NTA column again.

24. Once purity is verified, make the Size Exclusion Buffer:

    Size Exclusion Buffer:

    50 mM Tris (pH 8.0)

    150 mM KCl

    5% glycerol

    1 mM TCEP

25. Concentrate Ni-NTA flow-through fractions to 5–10 mL using 10-kDa molecular weight cut-off filters in the Sorvall ST 16R Centrifuge at 4,000*g*.

26. Apply protein to Superdex 200pg column at 1 mL/min. $HDAC8_{374}$ will elute after ~220–240 mL. An example of the final chromatogram for the size exclusion column is presented in Figure 6.

27. Use SDS-PAGE to verify the purity of enzyme in all observed peaks. Concentrate protein to 0.5–1 mL and determine concentration by measuring absorbance at 280 nm (molar absorptivity = 54,000 L mol^{-1} cm^{-1}; molecular weight = 41,000 kDa). A concentration of 10–15 mg/mL is sufficient for crystallization trials.

28. Flash-freeze protein in 50-μL aliquots using liquid nitrogen. Store protein at −80°C until needed.

4.4 Notes

$HDAC8_{374}$ is fully capable of catalyzing the hydrolysis of acetyllysine and behaves similarly to full-length wild-type human HDAC8 in activity assays and isothermal titration calorimetry experiments (Porter & Christianson, 2017).

5. Crystallization of HDAC8–Inhibitor Complexes

Currently, 47 structures of wild-type and mutant human HDAC8 have been deposited in the Protein Data Bank (Table 1). Of these, 37 are HDAC8-inhibitor complexes, but 23 of these are complexes with the pan-HDAC inhibitors SAHA, TSA, or M344. Many of these structures are clinically-identified mutants associated with Cornelia de Lange Syndrome. Of these 47 HDAC8 structures, the majority (57%) crystallize in the monoclinic space group $P2_1$. However, the orthorhombic space groups $P2_12_12_1$ or $P2_12_12$ are also observed (28%). Trigonal space group $P3_121$ (8%), trigonal space group $P3_2$ (4%), and tetragonal space group $P4_3$ (2%) are observed to a lesser extent. The $HDAC8_{374}$–Trapoxin A complex crystallizes in trigonal space group $P3_2$ (Porter & Christianson, 2017).

No crystal structure has been solved of exclusively unliganded HDAC8 despite more than a decade of study (although monomer C of the HDAC8-APHA complex lacks a bound inhibitor in its active site (Dowling et al., 2008)). This is attributed to the observation of different conformations of HDAC8 surface loops, suggesting that they are flexible and require restraint by inhibitor binding to facilitate crystallization (Decroos et al., 2015b). The flexibility of active site loops presumably influences the head-to-head packing of the commonly observed crystallographic dimer, which prevents the study of complexes with larger inhibitors.

In this section, we report the approach used to crystallize the $HDAC8_{374}$–Trapoxin A complex. Trapoxin A has the bulkiest capping group of any inhibitor studied to date with HDAC8, and the crystals of the enzyme-inhibitor complex diffract to the highest resolution (1.24 Å) measured to date for a complex with HDAC8. In principle, this approach can be used for the cocrystallization of any inhibitor complex with $HDAC8_{374}$.

5.1 Equipment

1. MiniSpin® plus centrifuge (Eppendorf #022620207)
2. Mosquito® crystallization robot (TTP Labtech)
3. 4°C cold room
4. EchoTherm™ Benchtop Incubator (Torrey Pines Scientific #IN55)
5. S8APO KL300 LED Microscope (Leica Microsystems)

5.2 Materials

1. $HDAC8_{374}$ protein
2. 10–40 mM Trapoxin A (Sigma Aldrich) in dimethyl sulfoxide (DMSO)

3. Size Exclusion Buffer: 50 mM Tris (pH 8.0), 150 KCl, 5% glycerol, 1 mM TCEP
4. Ultrafree®-MC centrifugal filter units (EMD Millipore UFC30GV00)
5. UV-transmissible polymer MRC 2-drop crystallization plates (Molecular Dimensions #MD11-00U0100)
6. 96-condition Crystallization Screens (Hampton Research)
    a. Index (#HR2-144)
    b. Crystal Screen (#HR-110) / Crystal Screen 2 (#HR2-112)
    c. PEGRx 1 (#HR2-082) / PEGRx 2 (#HR2-084)
    d. PEG/Ion (#HR2-126) / PEG/Ion 2 (#HR2-098)
7. Ethylene glycol (Sigma Aldrich #324558)

5.3 Procedure

1. Thaw the desired amount of HDAC8 from the −80°C freezer. Once thawed, keep protein on ice.
2. Thaw inhibitor solutions to room temperature. Do not store on ice. The melting temperature of DMSO is higher than that of water, so inhibitor solutions stored on ice will freeze.
3. In general, inhibitors are added to the enzyme solution with a final concentration of 2 mM. However, if the inhibitor is hydrophobic, it is wise to combine 1 μL of the 4 mM stock with 19 μL of size exclusion buffer to assess solubility. Continue to titrate in size exclusion buffer until the inhibitor has fully dissolved, and use that near-saturated inhibitor concentration instead of 2 mM. It can be helpful to dilute the 40 mM inhibitor stock so that the final screening solution is 5% DMSO. Do not exceed 5% DMSO.
4. $HDAC8_{374}$ may crystallize at both 5 and 10 mg/mL concentrations, so screening solutions should be made with both concentrations. Make these solutions by combining the constituents in the following order:
    a. $HDAC8_{374}$ (final concentration = 5 or 10 mg/mL)
    b. size exclusion buffer
    c. inhibitor stock in DMSO (final concentration = 2 mM unless otherwise determined)
5. Incubate samples on ice for 20–30 min. If precipitate is observed, the sample can either be filtered using an Ultrafree®-MC spin filter unit (1–2 min @ 14,000 rpm (13,000*g*) in the MiniSpin® plus centrifuge at 4°C) or centrifuged for 15 min at 14,000 rpm (13,000*g*) at 4°C.
6. Prepare the desired 96-well screens for crystallization trials. Generally, it is wise to screen four 96-well screens (see Materials section above) at both 4°C and

room temperature with two separate protein concentrations in each tray. This tests 1,536 conditions in the initial round of screening.

7. Set up crystallization screens using the Mosquito® crystallization robot with the following parameters:
   a. 80–100 μL reservoirs (a larger volume equilibrates more slowly)
   b. 100 nL precipitant drop
   c. 100 nL protein drop
   d. Store trays at either room temperature or 4°C
8. Needle-like crystals are commonly observed within 1–2 days. These can then be optimized by increasing/decreasing precipitant concentrations in 24-well screens.
9. For crystal harvesting, 20–25% ethylene glycol is generally a good cryoprotectant for flash-cooling and storage before collecting X-ray diffraction data.

5.4 Notes

The $HDAC8_{374}$ construct often crystallizes as needles in all of the screens mentioned in section 5.2. These can then be optimized using standard optimization approaches to generate three-dimensional crystals for structure determination. Conditions containing 20–25% of higher molecular weight polyethylene glycol polymers (MW ≥ 3,350 Da) have also yielded high quality crystals after 5–7 days of incubation at 4°C.

6. Summary

The approach described in this chapter for the analysis of crystal packing interactions and assessment of disordered polypeptide segments in a crystalline protein is generalizable for the analysis of any structure deposited in the Protein Data Bank (www.rcsb.org). As exemplified by the design of the $HDAC8_{374}$ construct, such analysis informs the design of alternative protein constructs that may exhibit alternative crystallization properties. Crystallization of the $HDAC8_{374}$ construct yields previously-unobserved crystal packing interactions in which active site loop conformations are not constrained by formation of a crystallographic dimer (Porter & Christianson, 2017). The $HDAC8_{374}$ construct may be useful in future studies focusing on the crystallization of complexes with large molecules.

Acknowledgements

This research was supported by NIH grant GM49758.

References

Abend A, & Kehat I (2015) Histone deacetylases as therapeutic targets – from cancer to cardiac disease. Pharmacology & Therapeutics, 147, 55–62. [PubMed: 25444758]

Allfrey VG, Faulkner R, & Mirsky AE (1964) Acetylation and methylation of histones and their possible role in the regulation of RNA synthesis. Proceedings of the National Academy of Sciences of the United States of America 51, 786–794. [PubMed: 14172992]

Ash DE, Cox JD, & Christianson DW (2000) Arginase: a binuclear manganese metalloenzyme. Metal Ions in Biological Systems, 37, 407–428. [PubMed: 10693141]

Aslanidis C, & de Jong PJ (1990) Ligation-independent cloning of PCR products (LIC-PCR). Nucleic Acids Research, 18, 6069–6074. [PubMed: 2235490]

Benedetti R, Conte M, & Altucci L (2015) Targeting histone deacetylases in diseases: where are we? Antioxidants & Redox Signaling, 23, 99–126. [PubMed: 24382114]

Castaneda CA, Wolfson NA, Leng KR, Kuo Y-M, Andrews AJ, & Fierke CA (2017) Histone deacetylase 8 substrate selectivity is determined by long- and short-range interactions leading to enhanced reactivity for full-length histone substrates compared to peptides. Journal of Biological Chemistry, 292, 21568–21577. [PubMed: 29109148]

Choudhary C, Weinert BT, Nishida Y, Verdin E, & Mann M (2014) The growing landscape of lysine acetylation links metabolism and cell signaling. Nature Reviews Molecular Cell Biology, 15, 536–550. [PubMed: 25053359]

Christianson DW, David PR, & Lipscomb WN (1987) Mechanism of carboxypeptidase A: hydration of a ketonic substrate analogue. Proceedings of the National Academy of Sciences of the United States of America, 84, 1512–1515. [PubMed: 3470737]

Cole KE, Dowling DP, Boone MA, Phillips AJ, & Christianson DW (2011) Structural basis of the antiproliferative activity of largazole, a depsipeptide inhibitor of the histone deacetylases. Journal of the American Chemical Society, 133, 12474–12477. [PubMed: 21790156]

Deardorff MA, Bando M, Nakato R, Watrin E, Itoh T, Minamino M, Saitoh K, Komata M, Katou Y, Clark D, Cole KE, De Baere E, Decroos C, Di Donarto N, Ernst S, Francey LJ, Gyftodimou Y, Hirashima K, Hullings M, Ishikawa Y, Jaulin C, Kaur M, Kiyono T, Lombardi PM, Magnaghi-Jaulin L, Mortier GR, Nozaki N, Petersen MB, Seimiya H, Siu VM, Suzuki Y, Takagaki K, Wilde JJ, Willems PJ, Prigent C, Gillessen-Kaesbach G, Christianson DW, Kaiser FJ, Jackson LG, Hirota T, Krantz ID, & Shirahige K (2012) HDAC8 mutations in Cornelia de Lange syndrome affect the cohesin acetylation cycle. Nature, 489, 313–317. [PubMed: 22885700]

Deardorff MA, Porter NJ, & Christianson DW (2016) Structural aspects of HDAC8 mechanism and dysfunction in Cornelia de Lange syndrome spectrum disorders. Protein Science, 25, 1965–1976. [PubMed: 27576763]

Decroos C, Bowman CM, Moser J-AS, Christianson KE, Deardorff MA, & Christianson DW (2014) Compromised structure and function of HDAC8 mutants identified in Cornelia de Lange Syndrome spectrum disorders. ACS Chemical Biology, 9, 2157–2164. [PubMed: 25075551]

Decroos C, Christianson NH, Gullett LE, Bowman CM, Christianson KE, Deardorff MA, & Christianson DW (2015a) Biochemical and structural characterization of HDAC8 mutants associated with Cornelia de Lange Syndrome spectrum disorders. Biochemistry, 54, 6501–6513. [PubMed: 26463496]

Decroos C, Clausen DJ, Haines BE, Wiest O, Williams RM, & Christianson DW (2015b) Variable active site loop conformations accommodate the binding of macrocyclic largazole analogues to HDAC8. Biochemistry, 54, 2126–2135. [PubMed: 25793284]

DeLano WL (2002) Pymol: an open-source molecular graphics tool. CCP4 Newsletter on Protein Crystallography, 40, 82–92.

Dokmanovic M, Clarke C, Marks PA (2007) Histone deacetylase inhibitors: overview and perspectives. Molecular Cancer Research, 5, 981–989. [PubMed: 17951399]

Dowling DP, Gantt SL, Gattis SG, Fierke CA, & Christianson DW (2008) Structural studies of human histone deacetylase 8 and its site-specific variants complexed with substrates and inhibitors. Biochemistry, 47, 13554–13563. [PubMed: 19053282]

Dowling DP, Gattis SG, Fierke CA, & Christianson DW (2010) Structures of metal-substituted human histone deacetylase 8 provide mechanistic inferences on biological function. Biochemistry, 49, 5048–5056. [PubMed: 20545365]

Ellmeier W, & Seiser C (2018) Histone deacetylase function in $CD4^+$ T cells. Nature Reviews Immunology 18, 617–634.

Falkenberg KJ, & Johnstone RW (2014) Histone deacetylases and their inhibitors in cancer, neurological diseases and immune disorders. Nature Reviews Drug Discovery, 13, 673–691. [PubMed: 25131830]

Ferrari L, Bragato C, Brioschi L, Spreafico M, Esposito S, Pezzotta A, Pizzetti F, Moreno-Fortuny A, Bellipanni G, Giordano A, Riva P, Frabetti F, Viani P, Cossu G, Mora M, Marozzi A, & Pistocchi A (2018) HDAC8 regulates canonical Wnt pathway to promote differentiation in skeletal muscles. Journal of Cellular Physiology, DOI: 10.1002/jcp.27341.

Ganai SA, Ramadoss M, & Mahadevan V (2016) Histone deacetylase (HDAC) inhibitors – emerging roles in neuronal memory, learning, synaptic plasticity and neural regeneration. Current Neuropharmacology, 14, 55–71. [PubMed: 26487502]

Gantt SL, Decroos C, Lee MS, Gullett LE, Bowman CM, Christianson DW, & Fierke CA (2016) General base-general acid catalysis in human histone deacetylase 8. Biochemistry, 55, 820–832. [PubMed: 26806311]

Gupta P, Reid RC, Iyer A, Sweet MJ, & Fairlie DP (2012) Towards isozyme-selective HDAC inhibitors for interrogating disease. Current Topics in Medicinal Chemistry, 12, 1479–1499. [PubMed: 22827519]

Gregoretti IV, Lee YM, & Goodson HV (2004) Molecular evolution of the histone deacetylase family: functional implication of phylogenetic analysis. Journal of Molecular Biology, 338, 17–31. [PubMed: 15050820]

Hai Y, & Christianson DW (2016) Histone deacetylase 6 structure and molecular basis of catalysis and inhibition. Nature Chemical Biology, 12, 741–747. [PubMed: 27454933]

Hornbeck PV, Zhang B, Murray B, Kornhauser JM, Latham V, & Skrzypek E (2015) PhosphoSitePlus, 2014: mutations, PTMs and recalibrations. Nucleic Acids Research, 43, D512–D520. [PubMed: 25514926]

Itazaki H, Nagashima K, Sugita K, Yoshida H, Kawamura Y, Yasuda Y, Matsumoto K, Ishi K, Uotani N, Nakai H, Terui A, Yoshimatsu S, Ikenishi Y, & Nakagawa Y (1990) Isolation and structural elucidation of new cyclotetrapeptides, Trapoxins A and B, having detransformation activities as antitumor agents. Journal of Antibiotics, 43, 1524–1532. [PubMed: 2276972]

Kaiser FJ, Ansari M, Braunholz D, Gil-Rodríguez MC, Decroos C, Wilde JJ, Fincher CT, Kaur M, Bando M, Amor DJ, Atwal PS, Bahlo M, Bowman CM, Bradley JJ, Brunner HG, Clark D, Del Campo M, Di Donato N, Diakumis P, Dubbs H, Dyment DA, Eckhold J, Ernst S, Ferreira JC, Francey LJ, Gehlken U, Guillén-Navarro E, Gyftodimou Y, Hall BD, Hennekam R, Hudgins L, Hullings M, Hunter JM, Yntema H, Innes AM, Kline AD, Krumina Z, Lee H, Leppig K, Lynch SA, Mallozzi MB, Mannini L, McKee S, Mehta SG, Micule I, Care4Rare Canada Consortium, Mohammed S, Moran E, Mortier GR, Moser JA, Noon SE, Nozaki N, Nunes L, Pappas JG, Penney LS, Pérez-Aytés A, Petersen MB, Puisac B, Revencu N, Roeder E, Saitta S, Scheuerle AE, Schindeler KL, Siu VM, Stark Z, Strom SP, Thiese H, Vater I, Willems P, Williamson K, Wilson LC, University of Washington Center for Mendelian Genomics, Hakonarson H, Quintero-Rivera F, Wierzba J, Musio A, Gillessen-Kaesbach G, Ramos FJ, Jackson LG, Shirahige K, Pié J, Christianson DW, Krantz ID, Fitzpatrick DR, & Deardorff MA (2014) Loss of function HDAC8 mutations cause a phenotypic spectrum of Cornelia de Lange Syndrome-like features, ocular hypertelorism, large fontanelle and X-linked inheritance. Human Molecular Genetics, 23, 2888–2900. [PubMed: 24403048]

Kanyo ZF, Scolnick LR, Ash DE, & Christianson DW (1996) Structure of a unique binuclear manganese cluster in arginase. Nature, 383, 554–557. [PubMed: 8849731]

Lombardi PM, Cole KE, Dowling DP, & Christianson DW (2011) Structure, mechanism, and inhibition of histone deacetylases and related metalloenzymes. Current Opinion in Structural Biology, 21, 735–743. [PubMed: 21872466]

Lopez JE, Haynes SE, Majmudar JD, Martin BR, Fierke CA (2017) HDAC8 substrates identified by genetically encoded active site photocrosslinking. J. Am. Chem. Soc 139, 16222–16227. [PubMed: 29035536]

Marek M, Shaik TB, Heimburg T, Chakrabarti A, Lancelot J, Ramos-Morales E, Da Veiga C, Kalinin D, Melesina J, Robaa D, Schmidtkunz K, Suzuki T, Holl R, Ennifar E, Pierce RJ, Jung M, Sippl W, & Romier C (2018) Characterization of Histone Deacetylase 8 (HDAC8) Selective Inhibition Reveals Specific Active Site Structural and Functional Determinants. Journal of Medicinal Chemistry, 61, 10000–10016. [PubMed: 30347148]

Olson DE, Udeshi ND, Wolfson NA, Pitcairn CA, Sullivan ED, Jaffe JD, Svinkina T, Natoli T, Lu X, Paulk J, McCarren P, Wagner FF, Barker D, Howe E, Lazzaro F, Gale JP, Zhang Y-L, Subramanian

A, Fierke CA, Carr SA, & Holson EB (2014) An unbiased approach to identify endogenous substrates of “histone” deacetylase 8. ACS Chem. Biol 9, 2210–2216. [PubMed: 25089360]

Pettersen EF, Goddard TD, Huang CC, Couch GS, Greenblatt DM, Meng EC, & Ferrin TE (2004) UCSF Chimera - A Visualization System for Exploratory Research and Analysis. Journal of Computational Chemistry, 25, 1605–1612. [PubMed: 15264254]

Porter NJ, Christianson NH, Decroos C, & Christianson DW (2016) Structural and functional influence of the glycine-rich loop G^{302}GGGY on the catalytic tyrosine of histone deacetylase 8. Biochemistry, 55, 6718–6729. [PubMed: 27933794]

Porter NJ, & Christianson DW (2017) Binding of the microbial cyclic tetrapeptide Trapoxin A to the class I histone deacetylase HDAC8. ACS Chemical Biology, 12, 2281–2286. [PubMed: 28846375]

Porter NJ, Mahendra A, Breslow R, & Christianson DW (2017) Unusual zinc-binding mode of HDAC6-selective hydroxamate inhibitors. Proceedings of the National Academy of Sciences of the United States of America, 114, 13459–13464. [PubMed: 29203661]

Sharma S, & Taliyan R (2015) Transcriptional dysregulation in Huntington’s disease: the role of histone deacetylases. Pharmacological Research 100, 157–169. [PubMed: 26254871]

Somoza JR, Skene RJ, Katz BA, Mol C, Ho JD, Jennings AJ, Luong C, Arvai A, Buggy JJ, Chi E, Tang J, Sang B-C, Verner E, Wynands R, Leahy EM, Dougan DR, Snell G, Navre M, Knuth MA, Swanson RV, McRee DE, & Tari LW (2004) Structural snapshots of human HDAC8 provide insights into the class I histone deacetylases. Structure, 12, 1325–1334. [PubMed: 15242608]

Tabackman AA, Frankson R, Marsan ES, Perry K, & Cole KE (2016) Structure of ‘linkerless’ hydroxamic acid inhibitor-HDAC8 complex confirms the formation of an isoform-specific subpocket. Journal of Structural Biology, 195, 373–378. [PubMed: 27374062]

Vannini A, Volpari C, Filocamo G, Casavola EC, Brunetti M, Renzoni D, Chakravarty P, Paolini C, De Francesco R, Gallinari P, Steinkühler C, & Di Marco S (2004) Crystal structure of a eukaryotic zinc-dependent histone deacetylase, human HDAC8, complexed with a hydroxamic acid inhibitor. Proceedings of the National Academy of Sciences of the United States of America, 101, 15064–15069. [PubMed: 15477595]

Vannini A, Volpari C, Gallinari P, Jones P, Mattu M, Carfí A, De Francesco R, Steinkühler C, & Di Marco S (2007) Substrate binding to histone deacetylases as shown by the crystal structure of the HDAC8-substrate complex. EMBO Reports, 8, 879–884 [PubMed: 17721440]

Wang Q, Zhang Y, Yang C, Xiong H, Lin Y, Yao J, Li H, Xie L, Zhao W, Yao Y, Ning ZB, Zeng R, Xiong Y, Guan KL, Zhao S, & Zhao GP (2010) Acetylation of metabolic enzymes coordinates carbon source utilization and metabolic flux. Science, 327, 1004–1007. [PubMed: 20167787]

Whitehead L, Dobler MR, Radetich B, Zhu Y, Atadja PW, Claiborne T, Grob JE, McRiner A, Pancost MR, Patnaik A, Shao W, Shultz MD, Tichkule R, Tommasi RA, Vash B, Wang P, & Stams T (2011) Human HDAC isoform selectivity achieved via exploitation of the acetate release channel with structurally unique small molecule inhibitors. Bioorganic & Medicinal Chemistry, 19, 4626–4634. [PubMed: 21723733]

Zhao S, Xu W, Jiang W, Yu W, Lin Y, Zhang T, Yao J, Zhou L, Zeng Y, Li H, Li Y, Shi J, An W, Hancock SM, He F, Qin L, Chin J, Yang P, Chen X, Lei Q, Xiong Y, & Guan KL (2010) Regulation of cellular metabolism by protein lysine acetylation. Science, 327, 1000–1004. [PubMed: 20167786]

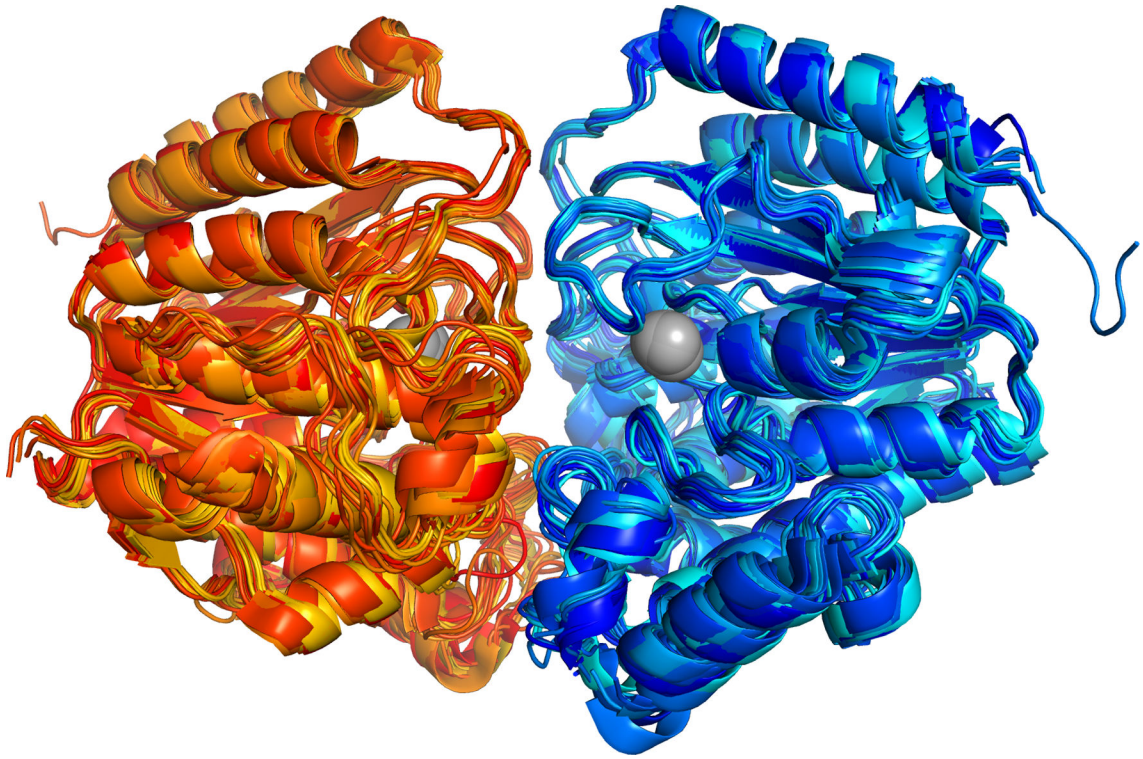

Figure 1.

Superposition of HDAC8 crystallographic dimer (monomer A = red/orange; monomer B = light/dark blue) in HDAC8–substrate and –inhibitor complexes. The superposition is comprised of crystal structures with PDB accession codes 1VKG, 2V5X, 3EZT, 3EWF, 3RQD, 4QA5, 4QA2, 4QA0, 4RN1, 5D1D, 5D1B, 5DC7, 5BWZ, 5FCW, 5THV, 5THT, and 5THS. The catalytic Zn^{2+} ions in each structure are shown as grey spheres.

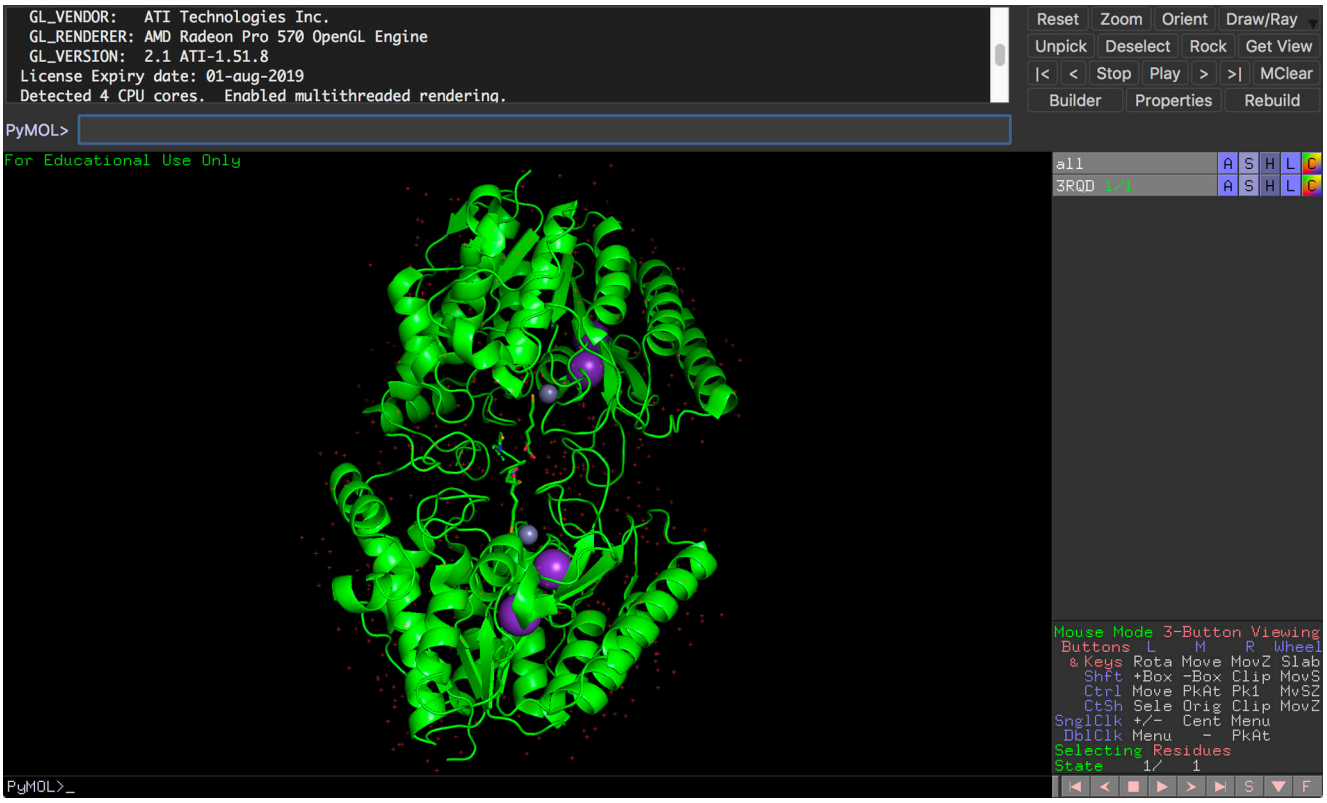

Figure 2.

Screenshot of Educational-Use-Only PyMOL window displaying PDB 3RQD. Protein is shown in green and the K^+ and Zn^{2+} ions are shown in purple and grey, respectively.

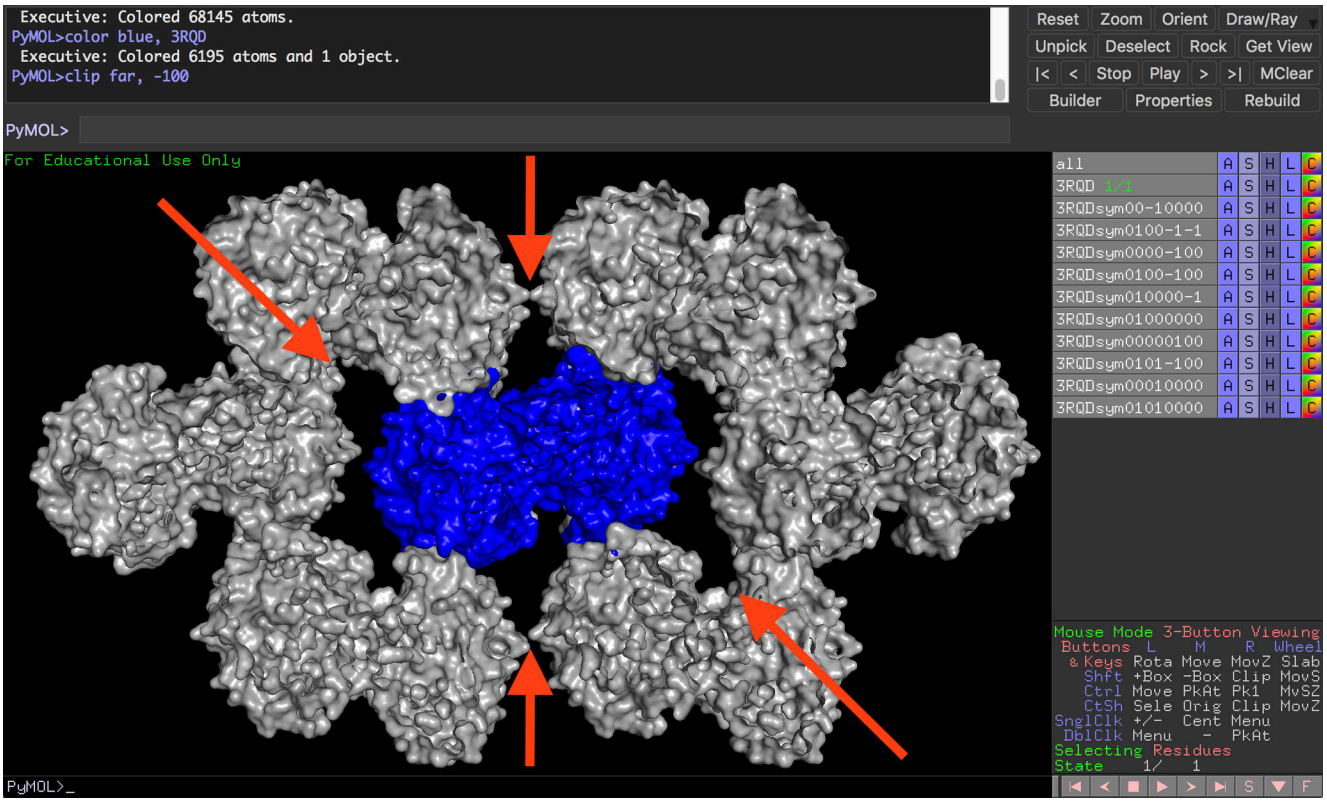

Figure 3.

Screenshot of symmetry mates displayed for PDB 3RQD. The initially loaded structure is shown in blue while the generated symmetry mates are shown in grey. Solvent voids within the crystal lattice surrounding the asymmetric unit are indicated by red arrows.

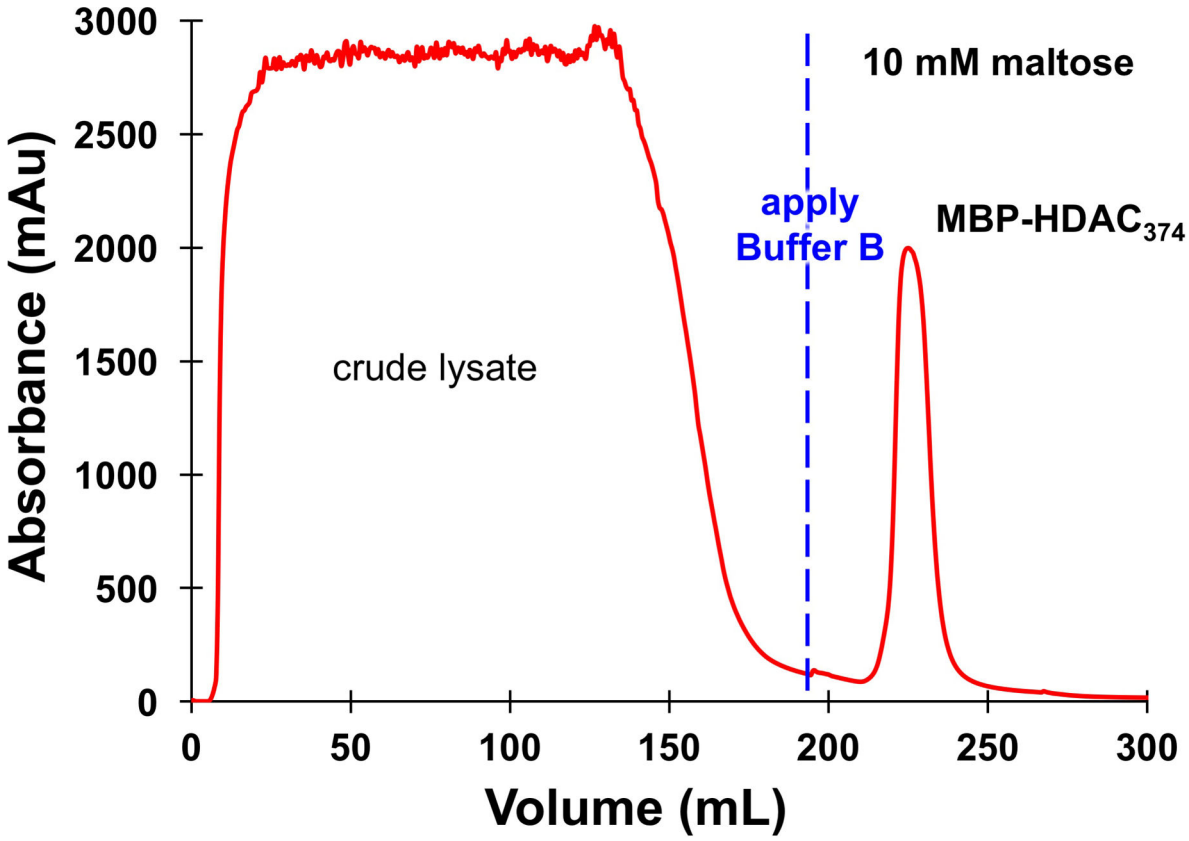

Figure 4.
FPLC chromatogram for the purification of MBP-HDAC8$_{374}$ from crude lysate using amylose resin.

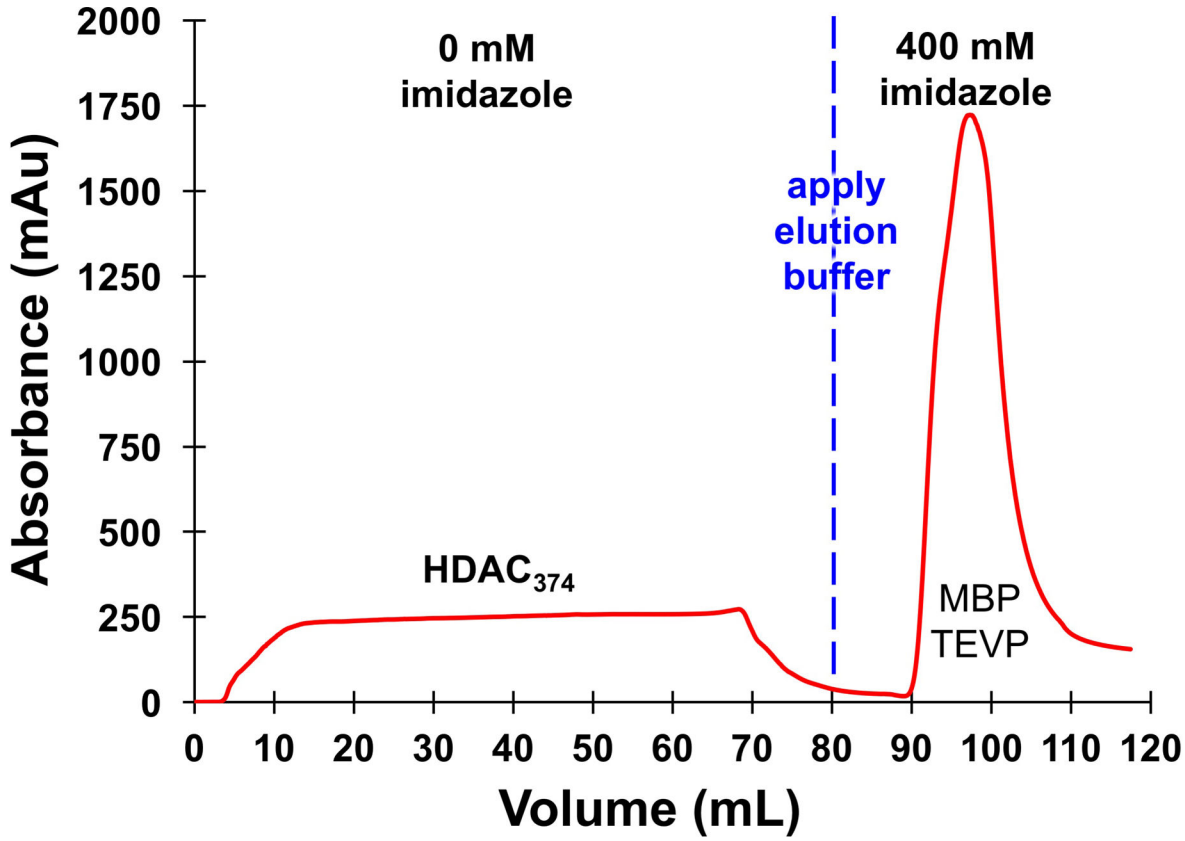

Figure 5.
FPLC chromatogram for the separation of $HDAC8_{374}$ from hexahistidine-tagged MBP and TEV protease (TEVP).

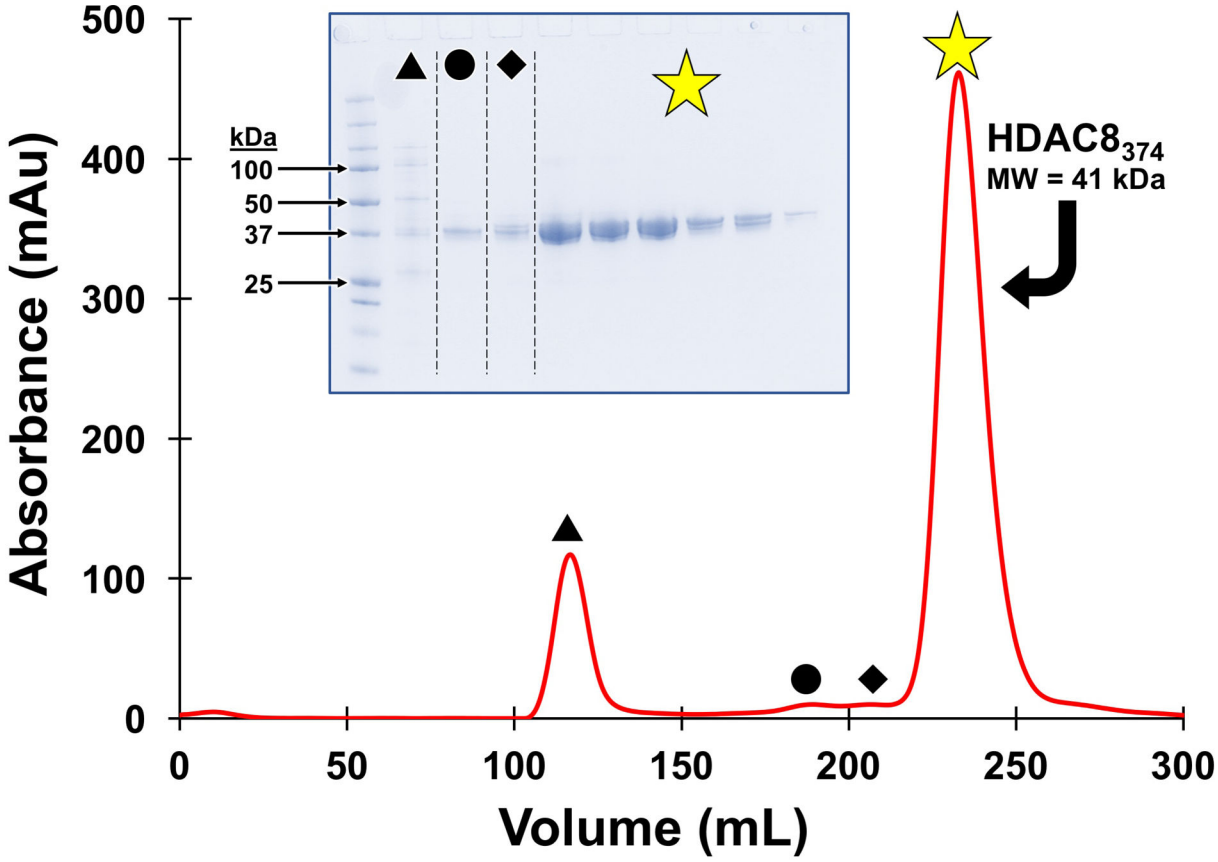

Figure 6.

FPLC chromatogram for the isolation of $HDAC8_{374}$ by size exclusion chromatography. Lanes of the inlaid gel correspond to peaks in the chromatogram as indicated.

Table 1.

Summary of space group parameters for crystalline HDAC8

PDB code	Resolution (Å)	Space Group	a (Å)	b (Å)	c (Å)	α (°)	β (°)	γ (°)
1W22	2.50		51.7	83.5	94.7	90	97.5	90
2V5W	2.00		52.3	151.8	57.6	90	117	90
3F06	2.55		55.9	85.9	94.8	90	98.1	90
3F07	3.30		88.4	90.2	92.1	90	94.7	90
3F0R	2.54		87.9	90.7	92.1	90	94.6	90
3EZP	2.65		55.3	91.8	94.6	90	93.6	90
3EZT	2.85		53.5	84.7	94.7	90	98.1	90
3MZ3	3.20		55.6	86.1	94.5	90	94	90
3SFF	2.00		57.8	53.7	61.3	90	109	90
3SFH	2.70		57.6	53.4	60.9	90	109.5	90
3RQD	2.14		54.1	88.0	93.7	90	101.6	90
4QA0	2.24		53.7	84.7	95.0	90	99.3	90
4QA1	1.92		98.4	82.6	105.6	90	102.2	90
4QA2	2.38	$P2_1$	53.0	84.1	94.4	90	98.6	90
4QA3	2.88		51.2	83.1	94.3	90	95.9	90
4QA6	2.05		51.8	85.1	94.49	90	97.6	90
4RN0	1.76		53.9	85.0	94.7	90	100.3	90
4RN1	2.18		54.0	85.1	95.4	90	100.2	90
4RN2	2.39		53.7	84.7	94.1	90	100.5	90
5D1B	2.90		52.2	83.0	98.4	90	102.7	90
5DC5	1.42		51.5	83.0	94.4	90	97.1	90
5BWZ	2.01		53.4	84.4	94.6	90	99.4	90
5FCW	1.98		53.4	84.5	94.3	90	100.8	90
5THS	1.90		53.2	84.4	94.6	90	99	90
5THT	2.41		97.7	83.8	99.8	90	91.7	90
5THU	1.95		53.5	83.9	98.4	90	101.8	90
5THV	1.87		53.0	82.9	94.6	90	99	90
3EW8	1.80		90.6	88.9	52.4	90	90	90
3MZ6	2.00	$P2_12_12$	91.6	87.6	52.5	90	90	90
3MZ7	1.90		91.8	88.4	52.5	90	90	90
1VKG	2.20		82.6	92.7	98.7	90	90	90
2V5X	2.25		84.3	98.7	110.5	90	90	90
3EWF	2.50		82.9	91.8	196.6	90	90	90
3MZ4	1.85		88.5	91.1	104.5	90	90	90
4QA5	1.76	$P2_12_12_1$	82.8	97.8	105.5	90	90	90
5D1C	1.42		83.0	97.9	104.7	90	90	90
5D1D	2.01		82.3	98.0	105.9	90	90	90
5DC6	1.55		82.3	98.2	104.3	90	90	90
5DC7	2.30		81.8	97.7	103.6	90	90	90

PDB code	Resolution (Å)	Space Group	a (Å)	b (Å)	c (Å)	α (°)	β (°)	γ (°)
5DC8	1.30		82.8	97.9	104.6	90	90	90
1T67	2.31	$P3_121$	80.6	80.6	105.5	90	90	120
1T69	2.91		80.7	80.7	105.6	90	90	120
4QA4	1.98		80.7	80.7	107.4	90	90	120
4QA7	2.31		80.4	80.4	106.1	90	90	120
5VI6	1.24	$P3_2$	51.0	51.0	116.5	90	90	120
6HSK	2.10		106.4	106.4	82.0	90	90	120
1T64	1.90	$P4_3$	81.1	81.1	114.2	90	90	90